LRP 549/96 June 1996

NORMAL CURVATURE, LOCAL MAGNETIC SHEAR AND PARALLEL CURRENT DENSITY IN TOKAMAKS AND TORSATRONS

W.A. Cooper

Submitted for publication
in Physics of Plasmas

Normal curvature, local magnetic shear and parallel current density in tokamaks and torsatrons

W. A. Cooper*

Centre de Recherches en Physique des Plasmas, Association Euratom-Confédération Suisse, Ecole Polytechnique Fédérale de Lausanne, CRPP-PPB, CH-1015 Lausanne, Switzerland

(June 12, 1996)

Abstract

Reversed magnetic shear is associated with large negative surface averaged parallel current densities that increase in magnitude towards the plasma edge and guarantee stability at large β in tokamaks. The surface averaged parallel current density is smaller and decreases in magnitude radially in conventional shear tokamaks. This results in much lower MHD stable β. The parallel current density in torsatrons is dominated by the Pfirsch-Schlüter currents, the global shear contributes negligibly to the local shear, and the β limits are comparable to that of a conventional tokamak. A simplistic evaluation of the local sign of the driving terms in the energy principle does not provide a useful guide to even qualitatively describe the MHD stability of a device. Ballooning instabilities concentrate in regions where the curvature is most destabilizing. The localization of these instabilities does not appear to depend on the sign of the interaction between the parallel current density and the local magnetic shear contribution to the driving term.

52.35.Py, 52.65.+z, 52.55.Hc

*E-mail: anthony.cooper@crpp.uhd.epfl.ch

I. INTRODUCTION

Reversed global magnetic shear operation in tokamaks has resulted in markedly improved plasma performance. To try to gain some understanding of the magnetohydrodynamic (MHD) stability properties, we investigate the ballooning stability of a 10 period torsatron, a reverse shear tokamak and a conventional shear tokamak. We consider the torsatron configuration as a base case, average the shape of its plasma-vacuum interface and apply its vacuum rotational transform to generate a reverse shear tokamak configuration with similar minor radius and apect ratio $\simeq 7$. We also examine this configuration with a conventional inverse transform profile that varies from unity at the magnetic axis to 2.5 at the plasma boundary. It is not really the purpose here to model specific experiments, but to to get a better comprehension of the underlying physics issues by choosing dimensions and profiles that can allow quantitative comparisons.

A new form of the MHD potential energy has recently been derived[1,2] which identifies a combination of the magnetic field line curvature, the local magnetic shear[3], and the parallel current density as essential driving mechanisms for MHD instabilities. The local magnetic shear properties have been previously analyzed in tokamaks.[4,5] Here, we evaluate all the quantities in question and attempt to identify which are the important characteristics that make the stability properties of the reverse shear tokamak superior to the conventional shear case and to the torsatron. In addition, we determine in each of the configurations we consider how the new factor in the energy principle driving term identified in Ref. 1, 2 affects the localization and triggering of instabilities.

The form of the energy principle developed in Ref. 1, 2 is displayed in Sec. II. The normal curvature in magnetic coordinates is presented in Sec. III. We derive the local magnetic shear in these coordinates in Sec. IV and the parallel current density in Sec. V. The ballooning stability calculations are discussed in Sec. VI. A Fourier analysis of the normal magnetic curvature, the local magnetic shear and the parallel current density is carried out in Sec. VII. The real space distributions of the factors in the energy principle driving term are shown in Sec. VIII, followed by Conclusions.

II. THE ENERGY PRINCIPLE

The MHD potential energy can be written as[1,2]

$$\delta W_p = \tfrac{1}{2}\int d^3x \Bigg(\left[Q - \left(\frac{p'(s)}{B^2} B - \sigma \frac{B \times \nabla s}{|\nabla s|^2} \right) (\xi \cdot \nabla s) \right]^2 + \Gamma p |\nabla \cdot \xi|^2 - [2p'(s)\kappa \cdot \nabla s + \sigma(S|\nabla s|^2 + \sigma B^2)] \frac{(\xi \cdot \nabla s)^2}{|\nabla s|^2} \Bigg) , \quad (1)$$

where s is the radial variable that labels the magnetic flux surfaces, p is the plasma pressure, Γ is the adiabatic index, prime ($'$) indicates the derivative of a flux surface quantity with respect to s, $\boldsymbol{B}$ is the magnetic field, $\sigma = \boldsymbol{j} \cdot \boldsymbol{B}/B^2$ is the parallel current density, $\boldsymbol{\kappa} = (\boldsymbol{b} \cdot \nabla)\boldsymbol{b}$ is the magnetic field line curvature, $\boldsymbol{b} = \boldsymbol{B}/B$ is the unit vector along the magnetic field lines, $S = -\boldsymbol{h} \cdot \nabla \times \boldsymbol{h}$ is the local magnetic shear[3] with $\boldsymbol{h} \equiv \boldsymbol{B} \times \nabla s/|\nabla s|^2$, $\boldsymbol{\xi}$ is the perturbed displacement vector, and $\boldsymbol{Q} = \nabla \times (\boldsymbol{\xi} \times \boldsymbol{B})$ is the perturbed magnetic field.

III. THE NORMAL CURVATURE

The interaction of the pressure gradient with the normal curvature constitutes one of the driving mechanisms of MHD instabilities.[1,2] This can be expressed in the Boozer magnetic coordinates[6] as

$$2p'(s)\sqrt{g}\boldsymbol{\kappa} \cdot \nabla s = \frac{p'(s)|\nabla s|^2}{B^2} \left[2\sqrt{g}p'(s) + \psi''(s)J(s) - \Phi''(s)I(s) + \psi'(s)J'(s) - \Phi'(s)I'(s) \right] - p'(s)\nabla s \cdot \nabla \sqrt{g} , \quad (2)$$

where $\sqrt{g}$ is the Jacobian of the transformation from Cartesian to magnetic coordinates, $2\pi\Phi(s)$ is the toroidal magnetic flux, $2\pi\psi(s)$ is the poloidal magnetic flux, $2\pi J(s)$ is the toroidal current within the flux surface, and $2\pi I(s)$ is the poloidal current flowing outside the flux surface. Expanding the last term and invoking useful relations valid in the magnetic coordinates,[7] we can write

$$2p'(s)\sqrt{g}\boldsymbol{\kappa} \cdot \nabla s = \frac{p'(s)|\nabla s|^2}{\sqrt{g}B^2}$$

$$\times \left\{ \sqrt{g}\Big[2\sqrt{g}p'(s) + \psi''(s)J(s) - \Phi''(s)I(s) + \psi'(s)J'(s) - \Phi'(s)I'(s)\Big] \right. \tag{3}$$
$$\left. - \sqrt{g}B^2\frac{\partial\sqrt{g}}{\partial s} - h_s\Big[I(s)\frac{\partial\sqrt{g}}{\partial\theta} + J(s)\frac{\partial\sqrt{g}}{\partial\phi}\Big] + B_s\Big[\psi'(s)\frac{\partial\sqrt{g}}{\partial\theta} + \Phi'(s)\frac{\partial\sqrt{g}}{\partial\phi}\Big]\right\},$$

where θ is the poloidal angle, ϕ is toroidal angle in the Boozer magnetic coordinates, and B_s and h_s are the radial components of the magnetic field and the vector $\boldsymbol{h}$ in the covariant representation, respectively.

IV. THE LOCAL MAGNETIC SHEAR

Another important component of the driving term of the energy principle is the local magnetic shear.[1,2] It can be expressed in the magnetic coordinates as

$$\sqrt{g}S = \psi'(s)\Phi''(s) - \Phi'(s)\psi''(s) - \sqrt{g}\boldsymbol{B}\cdot\boldsymbol{\nabla}h_s\,, \tag{4}$$

where the first two terms on the right hand side constitute the global magnetic shear, while the last term corresponds to the contribution that makes the magnetic shear vary locally on a magnetic surface. Thus, h_s constitutes the flux surface varying component of the local magnetic shear integrated along the field lines. It can be expressed as

$$h_s = \frac{\sqrt{g}B^2}{\Phi'(s)|\boldsymbol{\nabla}s|^2}\Big[\frac{g_{s\theta}}{\sqrt{g}} - \frac{J(s)B_s}{\sqrt{g}B^2}\Big]\,, \tag{5}$$

where $g_{s\theta}$ is one of the metric elements. From the Fourier decomposition of Eq. (4), we obtain the amplitudes

$$(\sqrt{g}S)_{00}(s) = \psi'(s)\Phi''(s) - \Phi'(s)\psi''(s) \tag{6}$$

and

$$(\sqrt{g}S)_{mn}(s) = -[m\psi'(s) - nL\Phi'(s)]h_{smn}(s)\,, \tag{7}$$

where

$$h_{smn}(s) = \frac{2L}{4\pi^2}\int_0^{\frac{2\pi}{L}} d\phi \int_0^{2\pi} d\theta h_s(s,\theta,\phi)sin(m\theta - nL\phi)\,, \tag{8}$$

m is the poloidal mode number, n is the toroidal mode number per period, and L is the number of field periods. For axisymmetry, we have $L = 1$.

V. THE PARALLEL CURRENT DENSITY

The third relevant term that can contribute to the driving mechanism of MHD instabilities is the parallel current density. It is evaluated by invoking the condition of charge conservation $\nabla \cdot \boldsymbol{j} = 0$ and MHD force balance $\nabla p = \boldsymbol{j} \times \boldsymbol{B}$. Decomposing the current density $\boldsymbol{j}$ into components aligned with $\boldsymbol{B}$ and perpendicular to it, one can derive the relation

$$\sqrt{g}\boldsymbol{B} \cdot \nabla \sigma = \frac{p'(s)}{\sqrt{g}B^2}\left[I(s)\frac{\partial \sqrt{g}}{\partial \theta} + J(s)\frac{\partial \sqrt{g}}{\partial \phi}\right] \tag{9}$$

in the magnetic coordinates. This procedure to evaluate the parallel current density is specially important for the determination of MHD stability of 3D systems.[8–10] This relation, however, specifies the parallel current density upto a constant on each flux surface. This constant is obtained from a direct decomposition of $\boldsymbol{j} \cdot \boldsymbol{B}/B^2$. Fourier analysis of $\boldsymbol{j} \cdot \boldsymbol{B}/B^2$ yields

$$\sigma_{mn}(s) = \frac{p'(s)}{\sqrt{g}B^2}\left[\frac{mI(s) - nLJ(s)}{m\psi'(s) - nL\Phi'(s)}\right]\sqrt{g}_{mn} \,. \tag{10}$$

This is valid for all (m, n) pairs except for $(m = 0, n = 0)$. The flux surface constant component is

$$\sigma_{00}(s) = \frac{J(s)I'(s) - I(s)J'(s)}{\sqrt{g}B^2} \,. \tag{11}$$

One of the properties of the magnetic coordinates is that $\sqrt{g}B^2 = \psi'(s)J(s) - \Phi'(s)I(s)$ is constant on a flux surface.[6]

The interaction of the parallel current density with itself and with the local shear that can compete with the normal curvature to drive instability is $\sigma(\sqrt{g}S|\nabla s|^2 + \sigma\sqrt{g}B^2)$. However, as discussed in Ref. 1, 2, this factor also appears in the stabilizing term of the energy principle, thus its impact as a source of instability is not clear cut. One of the aims of this work is to evaluate how it affects MHD stability. For this purpose, we shall examine the stability properties of a 10 field period torsatron and compare it with a tokamak of similar aspect ratio and average minor radius.

VI. BALLOONING STABILITY ANALYSIS

As a first step, we evaluate the ballooning stability of the configurations that we are considering. The MHD equilibria are obtained with the VMEC code.[11] In these calculations, we employ 96 radial intervals. We compute equilibria 1) for a tokamak with a fixed conventional rotational transform profile given by

$$\iota(s) = 1 - 0.6s^2 \,, \tag{12}$$

2) for a 10 period torsatron with a transform profile given by

$$\iota(s) = 0.352 + 0.5077s - 0.1595s^2 + 0.4942s^3 \,, \tag{13}$$

which fits almost exactly its vacuum transform profile, 3) for the tokamak, but prescribing the torsatron vacuum transform to produce a reversed shear case, and 4) for the torsatron with vanishing toroidal current within each flux surface, at volume average $\beta = 2\%$. The corresponding inverse rotational transform profiles are described in Fig. 1. The pressure profile is given by

$$p(s) = p(0)(1 - s)^2 \,, \tag{14}$$

where we adjust p(0) to obtain the desired value of β. The ballooning stability analysis is carried out in the Boozer magnetic coordinates[6] using the modules of the TERPSICHORE code[15] that evaluate local MHD stability. The ballooning eigenvalue profiles are shown in Fig. 2. The tokamak with conventional transform profile is unstable for $s \lesssim 0.6$ at $\beta = 2\%$. At this β, the torsatron is also unstable. In the zero toroidal current case, the region $0.42 < s < 0.68$ is unstable and in the fixed vacuum transform case, the region $0.36 < s < 0.72$ is unstable. The most unstable ballooning eigenstructures are localized on the outside edge of the prolate up-down symmetric toroidal cross section that is positioned at the half period. In contrast, the reversed shear tokamak is very stable and β has to increase to 13.4% to become marginally unstable about $s \simeq 0.7$.

VII. FOURIER ANALYSIS

A. Pressure gradient and normal curvature interaction

The Fourier amplitudes of the 4 dominant components of the normal curvature term described in Sec. III are displayed in Fig. 3 for the conventional shear tokamak, in Fig. 4 for the reverse shear tokamak, and in Fig. 5 for the 10 period torsatron with vacuum transform at $\beta = 2\%$. The tokamak configuration is dominated by the $(m = 1, n = 0)$ component, with a profile that is similar in shape and in magnitude irrespective of the sign of the global magnetic shear. The normalization in the Boozer coordinates with negative Jacobian that we have applied implies that negative amplitudes are destabilizing. The curvature in the torsatron with vacuum transform is completely dominated by helical $n = 1$ components, of which the $m = 2 - 4$ amplitudes are positive and the $m = 1$ is negative. The net effect is that the pressure gradient-normal curvature interaction is most destabilizing at the outer side of the prolate up-down symmetric toroidal cross section. The normal curvature analysis of the current-free torsatron case differs only in minor details.

B. Local magnetic shear

The Fourier decomposition of the local magnetic shear term $s\sqrt{g}S$ shows that for the tokamak, the global shear [the $(m = 0, n = 0)$ component] dominates, while the helical $n \neq 0$ components are the most important in the torsatron. In contrast with the characteristic behavior of the normal curvature, there is a more significant difference in the local magnetic shear properties between the conventional and reverse shear tokamak cases. In the conventional tokamak the global shear is positive with a subdominant $(m = 1, n = 0)$ component that reduces the shear on the outside and increases it on the inside of a toroidal cross section. This is shown in Fig. 6. In the reverse shear case, the global shear is negative and the subdominant $(m = 1, n = 0)$ component makes the local shear less negative on the outside and more negative on the inside of a toroidal cross section for $s > 0.4$ as shown in Fig. 7. The global shear plays no significant role

in the torsatron which has positive $(m = 2, n = 1)$ and $(m = 3, n = 2)$ components that increase radially and a roughly constant negative $(m = 1, n = 1)$ component. The 4 dominant amplitudes are displayed in Fig. 8. The zero current case differs mainly due to a positive $(m = 0, n = 1)$ contribution that peaks at $s \simeq 0.4$.

C. Parallel current density

The 4 dominant Fourier amplitudes of the parallel current density are plotted as a function of s for the conventional shear tokamak in Fig. 9, for the reverse shear tokamak in Fig. 10, and for the the torsatron with fixed vacuum transform in Fig. 11. In the conventional shear tokamak, the $(m = 0, n = 0)$ component is dominant, negative in the central region of the plasma, and decreases in magnitude radially becoming positive near the edge with the rotational transform profile we have prescribed. In the reverse shear tokamak, the $m > 0$ components are similar to those of the conventional tokamak. The $(m = 0, n = 0)$ component is negative everywhere increasing in magnitude from the center to the edge. The parallel current density in the torsatron is dominated by the axisymmetric components $(n = 0)$. The helical components $(n \neq 0)$ are important only very locally about resonant magnetic surfaces. The current-free torsatron is similar, except that the $(m = 0, n = 0)$ component vanishes by definition because we prescribe $J(s) = J'(s) = 0$. The shape of the σ_{00} profile is the distinguishing feature of the reverse shear tokamak.

VIII. REAL SPACE DISTRIBUTIONS

A. Conventional and reverse shear tokamak comparison

The magnetic field line curvature is negative and destabilizing at the outside edge of the flux surfaces in a tokamak. The global magnetic shear properties do not significantly affect its magnitude or distribution. We evaluate $2p'(s)\sqrt{g}\boldsymbol{\kappa} \cdot \boldsymbol{\nabla} s$ on a cross section of constant toroidal angle in Fig. 12a for the conventional shear tokamak case and in Fig. 12b for the reverse shear

tokamak case at $\beta = 2\%$. The differences in the normal magnetic curvature distribution are essentially minor. The maximum and minimum values of $2p'(s)\sqrt{g}\boldsymbol{\kappa} \cdot \boldsymbol{\nabla} s$ are 0.12 and -0.42 for reverse shear, respectively, and 0.15 and -0.32 for conventional shear, respectively. The distribution of $\sigma(\sqrt{g}S|\boldsymbol{\nabla} s|^2 + \sigma\sqrt{g}B^2)$ which constitutes the residual contribution to the destabilizing term in the energy principle is diplayed in Fig. 12c for the conventional shear tokamak and in Fig. 12d for the reverse shear tokamak at $\beta = 2\%$. In the standard tokamak, this distribution has a similar shape to that of the normal magnetic curvature and it is negative in the region of destabilizing curvature. The minimum value approaches -1.9. The dominant contribution, specially in the relevant region of weak curvature, comes from $\sigma^2\sqrt{g}B^2$ and is displayed in Fig. 12e. The $\sigma\sqrt{g}S|\boldsymbol{\nabla} s|^2$ contribution is important in a uniform narrow layer around the edge of the plasma and has a positive value close to 0.3 in the destabilizing curvature region. The $\sigma(\sqrt{g}S|\boldsymbol{\nabla} s|^2 + \sigma\sqrt{g}B^2)$ pattern in the reversed shear tokamak case is distinctly different. It is negative throughout, most noticeably in the vicinity of the plasma edge where it has a value of -5.23 as seen in Fig. 12d. In the relevant region of weak curvature, its value is somewhat more negative, ~ -2.3, than in the conventional shear device. A comparison reveals that $\sigma^2\sqrt{g}B^2$ (shown in Fig. 12f) also dominates over $\sigma\sqrt{g}S|\boldsymbol{\nabla} s|^2$ in this case, but the magnitudes are much larger than with conventional shear. In the destabilizing curvature domain, we have $\sigma^2\sqrt{g}B^2 \sim -3.8$ and $\sigma\sqrt{g}S|\boldsymbol{\nabla} s|^2 \sim 1.5$. The large negative values extending to the edge can be attributed directly to the shape of the σ_{00} profile shown in Fig. 10.

Analyzing the magnitudes of the two contributions of the driving term in the energy principle, one would be lead to conclude that the edge region should be strongly unstable in the reverse shear tokamak. It is not. Furthermore, concentrating on the neighborhood of most negative normal curvature, we find that the sum of the driving term contributions would be $(-0.4-2.3 = -2.7)$ for reverse shear and $(-0.3-1.9 = -2.2)$ for conventional shear. Thus, we would anticipate from just an examination of the driving term alone that the reverse shear case would be more unstable than the conventional shear case, contrary to what we obtain from the computation of ballooning modes. This clearly suggests that the contributions of the local magnetic shear and the parallel current density in the stabilizing first term of the energy principle outweigh their

destabilizing impact in the last term. The net effect in the tokamak appears to be that the more negative $\sigma(\sqrt{g}S|\nabla s|^2 + \sigma\sqrt{g}B^2)$ becomes, the more stabilizing its influence is. Increasing β in the reverse shear tokamak causes $\sigma^2\sqrt{g}B^2$ to become more negative (minimum value:-50) and $\sigma\sqrt{g}S|\nabla s|^2$ to become more positive (maximun value:40). They combine to make $\sigma(\sqrt{g}S|\nabla s|^2 + \sigma\sqrt{g}B^2)$ effectively more negative at higher β, but the rate of increase in the magnitude of $2p'(s)\sqrt{g}\boldsymbol{\kappa}\cdot\nabla s$ is faster which eventually destabilizes the ballooning mode at $\beta = 13.4\%$.

An interesting feature is that the contours of constant poloidal angle in the tokamak with conventional shear fan out on the outside edge of the plasma all the way to the boundary. In the reverse shear case, they radially fan out more rapidly at first, but cease to diverge further at about half radius. The behavior in the torsatron is similar as can be seen in the figures of the next section.

B. Torsatron

The pressure gradient-normal curvature interaction $2p'(s)\sqrt{g}\boldsymbol{\kappa}\cdot\nabla s$ is shown on two toroidal cross sections in Fig. 13a for the torsatron with fixed vacuum transform at $\beta = 2\%$. The destabilizing curvature concentrates on the outer side of the prolate up-down symmetric cross section located halfway within one period that appears in the foreground of Fig. 13a. It is on this plane that the most unstable ballooning modes on each surface concentrate. The minimum value of $2p'(s)\sqrt{g}\boldsymbol{\kappa}\cdot\nabla s$ is -1.304. The oblate up-down symmetric cross section at the beginning (and end) of a field period appears partially concealed in the background. The $\sigma(\sqrt{g}S|\nabla s|^2+\sigma\sqrt{g}B^2)$ pattern on the same cross sections is shown in Fig. 13b. The location of its maximum value of 3.2 roughly coincides with that where $2p'(s)\sqrt{g}\boldsymbol{\kappa}\cdot\nabla s$ is most negative. Its most negative value of -5.4 lies at midradius on the outside edge of the oblate up-down symmetric cross section. Adding up the contributions of $2p'(s)\sqrt{g}\boldsymbol{\kappa}\cdot\nabla s$ and $\sigma(\sqrt{g}S|\nabla s|^2 + \sigma\sqrt{g}B^2)$ would predict the most unstable domain to concentrate on the outer side of the oblate rather than the prolate up-down symmetric cross section. The torsatron ballooning stability results we have obtained suggest that the net effect of the local shear and parallel current density contributions to the

different terms of the energy principle is such that regions where $\sigma(\sqrt{g}S|\nabla s|^2 + \sigma\sqrt{g}B^2)$ is positive are destabilizing and where it is negative are stabilizing. However, mode structures localize preferentially where the curvature is destabilizing and $\sigma(\sqrt{g}S|\nabla s|^2 + \sigma\sqrt{g}B^2)$ competes with $2p'(s)\sqrt{g}\boldsymbol{\kappa}\cdot\nabla s$ to determine at what β these are triggered.

For completeness, we show the distribution of $\sigma\sqrt{g}S|\nabla s|^2$ in Fig. 13c and $\sigma^2\sqrt{g}B^2$ in Fig. 13d, $\sqrt{g}S|\nabla s|^2$ in Fig. 13e, and σ in Fig. 13f. Clearly, the distribution of $\sigma(\sqrt{g}S|\nabla s|^2 + \sigma\sqrt{g}B^2)$ is more closely aligned with that of $\sigma\sqrt{g}S|\nabla s|^2$. In the weakest curvature region, $\sigma\sqrt{g}S|\nabla s|^2 > |\sigma^2\sqrt{g}B^2|$ to guarantee that their sum is positive. On the oblate up-down symmetric plane both contributions are negative on the outside. This is different from the tokamak where $\sigma^2\sqrt{g}B^2$ is dominant. The local shear pattern $\sqrt{g}S|\nabla s|^2$ alone does not appear to reveal distinctive features that elucidate the conditions that trigger and localize MHD instabilities. It is only through its interaction with the parallel current density that we gain any intuitive understanding about its impact. In particular, the regions of vanishing local shear do not coincide with the ballooning unstable region. The $\sigma^2\sqrt{g}B^2$ and σ distributions are consistent with a parallel current density dominated by the $(m = 1, n = 0)$ component as shown in Fig. 11. Localized resonant features in the parallel current density at rational surfaces are in evidence in these figures, in particular, the $(m = 14, n = 1)$ component at $s \approx 0.6$.

IX. CONCLUSIONS

We have examined the ideal MHD stability of a torsatron with vanishing toroidal current and with fixed vacuum rotational transform, a reverse shear tokamak with the torsatron vacuum transform, and a tokamak with a conventional shear transform profile. The reversed shear tokamak remains stable upto $\beta = 13.4\%$, while the conventional shear tokamak is unstable at $\beta = 2\%$. The torsatron stability properties are comparable to that of the conventional shear tokamak rather than the reversed shear counterpart despite having imposed identical global magnetic shear. We have investigated the interaction of the pressure gradient with the normal magnetic curvature, the local magnetic shear, the parallel current density, and their mutual

interactions which form the basis of the driving term of the energy principle to attempt to elucidate what are the characteristic features that distinguish the favorable stability properties of the reversed shear tokamak.

The destabilizing normal curvature is localized at the outside edge of each flux surface in the tokamak and is similar in magnitude and distribution regardless of the sign of the global shear. In the torsatron, the normal curvature is dominated by the helical Fourier components ($n = 1$) and is most unstable at the outside edge of the prolate up-down symmetric toroidal cross section. The local magnetic shear is dominated by the global shear in the tokamak, except in the vicinity of the magnetic axis. It is thus positive for the conventional shear tokamak and negative for the reverse shear case. A subdominant $m = 1, n = 0$ Fourier component enhances the contribution of the global shear to the local shear on the inside edge and reduces it on the outside edge of the flux surfaces. In the torsatron, the local magnetic shear is dominated by helical components and the effect of the global shear is negligible. The $m = 0, n = 0$ component of the parallel current density is negative and increases in magnitude radially in the reverse shear tokamak. This appears to be one of the essential features that characterizes its favorable stability properties. This component is negative near the axis and decreases in magnitude towards the edge with standard global shear. The flux surface average of the parallel current is imposed to vanish with zero net toroidal current in the torsatron, or is small compared to other components if the vacuum transform is prescribed.

The reversed shear tokamak has the most negative values of the $\sigma(\sqrt{g}S|\nabla s|^2 + \sigma\sqrt{g}B^2)$ component of the energy principle. In conventional shear tokamaks, this term is also negative, but of smaller magnitude, and in the torsatron it is positive in the region of destabilizing magnetic field line curvature. Negative values alone do not guarantee stability, but we can conclude that the more negative they are the more stabilizing is the impact. This contradicts what we would expect from a simpleminded quantitative analysis of just the instability driving terms of the energy principle which would predict the reverse shear tokamak to be more unstable than its conventional shear counterpart and that unstable modes concentrate at the outer edge of the

oblate up-down cross section in the torsatron. The large negative values of $\sigma(\sqrt{g}S|\nabla s|^2+\sigma\sqrt{g}B^2)$ in the reverse shear tokamak are directly attributable to the shape and magnitude of $\sigma_{00}(s)$ profile. Analyzing the averaged parallel current density, we conclude that negative $J'(s)$ in regions of large $p'(s)$ enhances MHD stability. The normalization we have adopted has negative $J(s)$, thus negative $J'(s)$ corresponds to a hollow current profile. The large currents near the boundary could destabilize external kink modes in the absence of a close fitting conducting wall.

ACKNOWLEDGMENTS

This research was partially sponsored by the Fonds National Suisse de la Recherche Scientifique and by Euratom. We thank Dr. S.P. Hirshman for use of the VMEC equilibrium code, Dr. S. Merazzi for use of the BASPL 3D graphics package, and Dr. T.M. Tran, S. Bernel, and P. Le Meur for assistance with the graphics.

REFERENCES

[1] R.L. Dewar, D.A. Monticello, and W.N.C. Sy, Phys. Fluids **27**, 1723 (1984).

[2] J.M. Greene, Phys. Plasmas **3**, 8 (1996).

[3] J.M. Greene and J.L. Johnson, Plasma Phys. **10**, 729 (1968).

[4] J.M. Greene and M.S. Chance, Nucl. Fusion **21**, 453 (1981).

[5] J.L.V. Lewandowski and M. Persson, Plasma Phys. Contr. Fusion **37**, 1199 (1995).

[6] A.H. Boozer, Phys. Fluids **23**,904 (1980).

[7] W.A. Cooper, Plasma Phys. Contr. Fusion **34**, 1011 (1992).

[8] J. Nührenberg and R. Zille, *Equilibrium and stability of low-shear stellarators* in "Theory of Fusion Plasmas," A. Bondeson, E. Sindoni, and F. Troyon eds. (Soc. Ital. Fisica – Editrice Compositori, Bologna, 1988) pp. 3–23.

[9] H.J. Gardner and B.D. Blackwell, Nucl. Fusion **32**, 2009 (1992).

[10] R. Moeckli and W.A. Cooper, Nucl. Fusion **33**, 1899 (1993).

[11] S.P. Hirshman and O. Betancourt, J. Comput. Phys. **96**, 99 (1991).

[12] J.W. Connor, R.J. Hastie, and J.B. Taylor, Proc. R. Soc. London A **365**, 1 (1979).

[13] D. Correa-Restrepo, Z. Naturforsch. **33a**, 789 (1978).

[14] R.L. Dewar and A.H. Glasser, Phys. Fluids **26**, 3038 (1983).

[15] D.V. Anderson, W.A. Cooper, R. Gruber, S. Merazzi, and U. Schwenn, Int. J. Supercomp. Appl. **4**, 34 (1990).

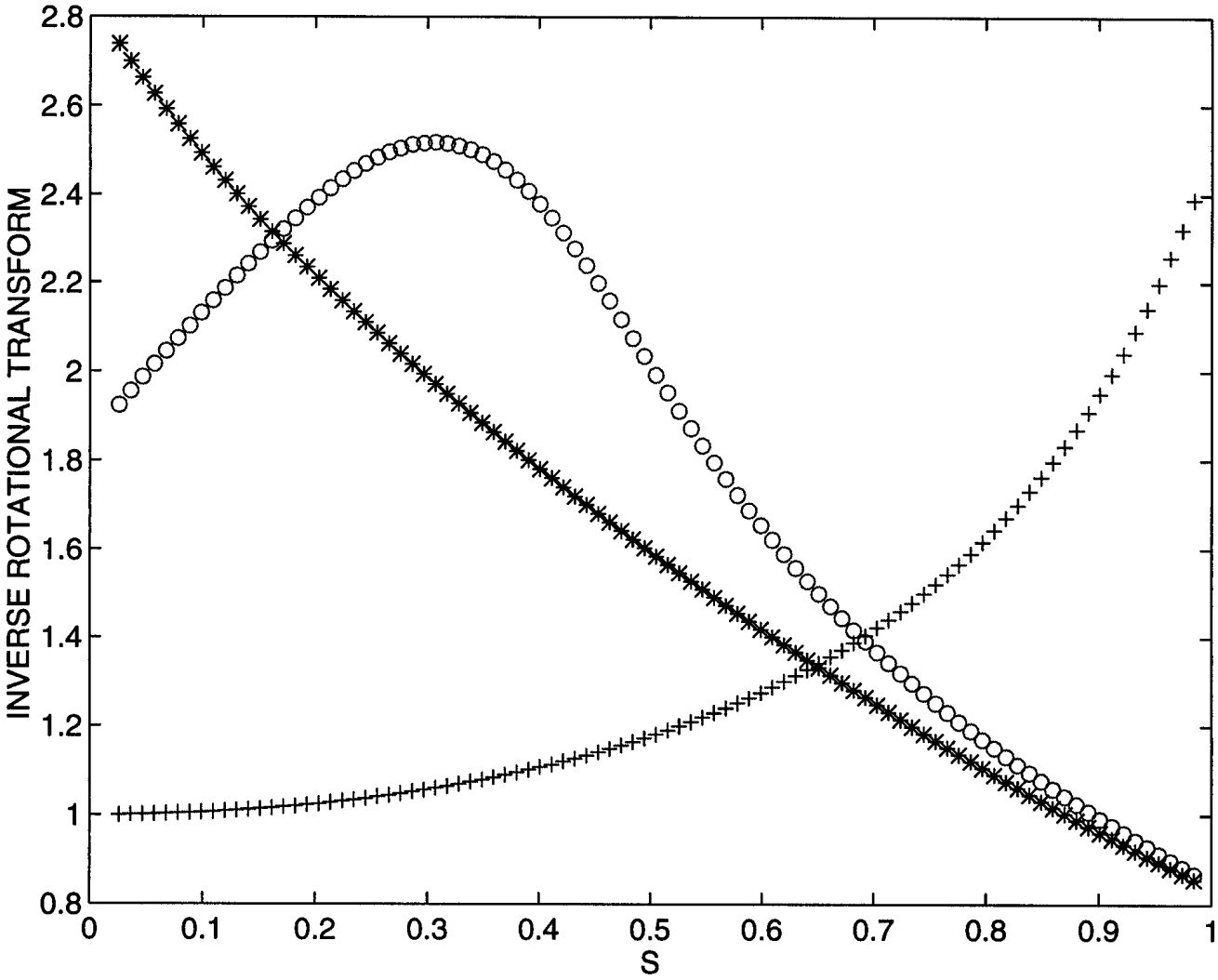

FIG. 1. The inverse rotational transform profiles for a conventional tokamak (+), for a 10 period torsatron in vacuum (∗), and for a 10 period torsatron with zero net toroidal current at $\beta = 2\%$ (o).

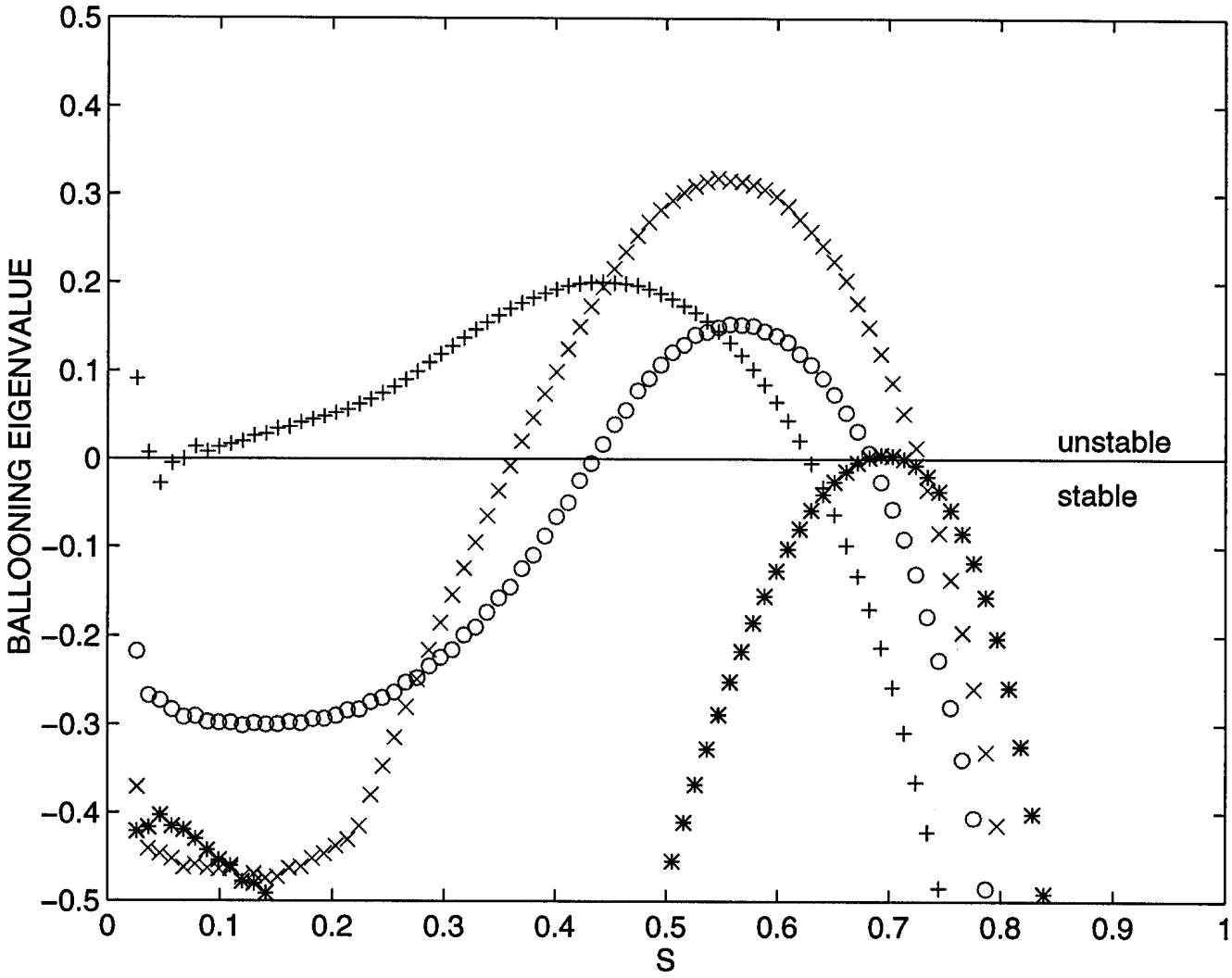

FIG. 2. The ballooning eigenvalues as a function of the radial variable s for a tokamak at $\beta = 2\%$ with a conventional rotational transform profile (+), a torsatron at $\beta = 2\%$ with zero net toroidal current (o), a torsatron at $\beta = 2\%$ with a fixed rotational transform profile corresponding to its vacuum profile ($\times$), and a reverse shear tokamak at $\beta = 13.4\%$ with the torsatron vacuum rotational profile ($*$). Positive values are unstable and negative values are stable. Eigenvalues smaller than -0.5 are omitted from the figure.

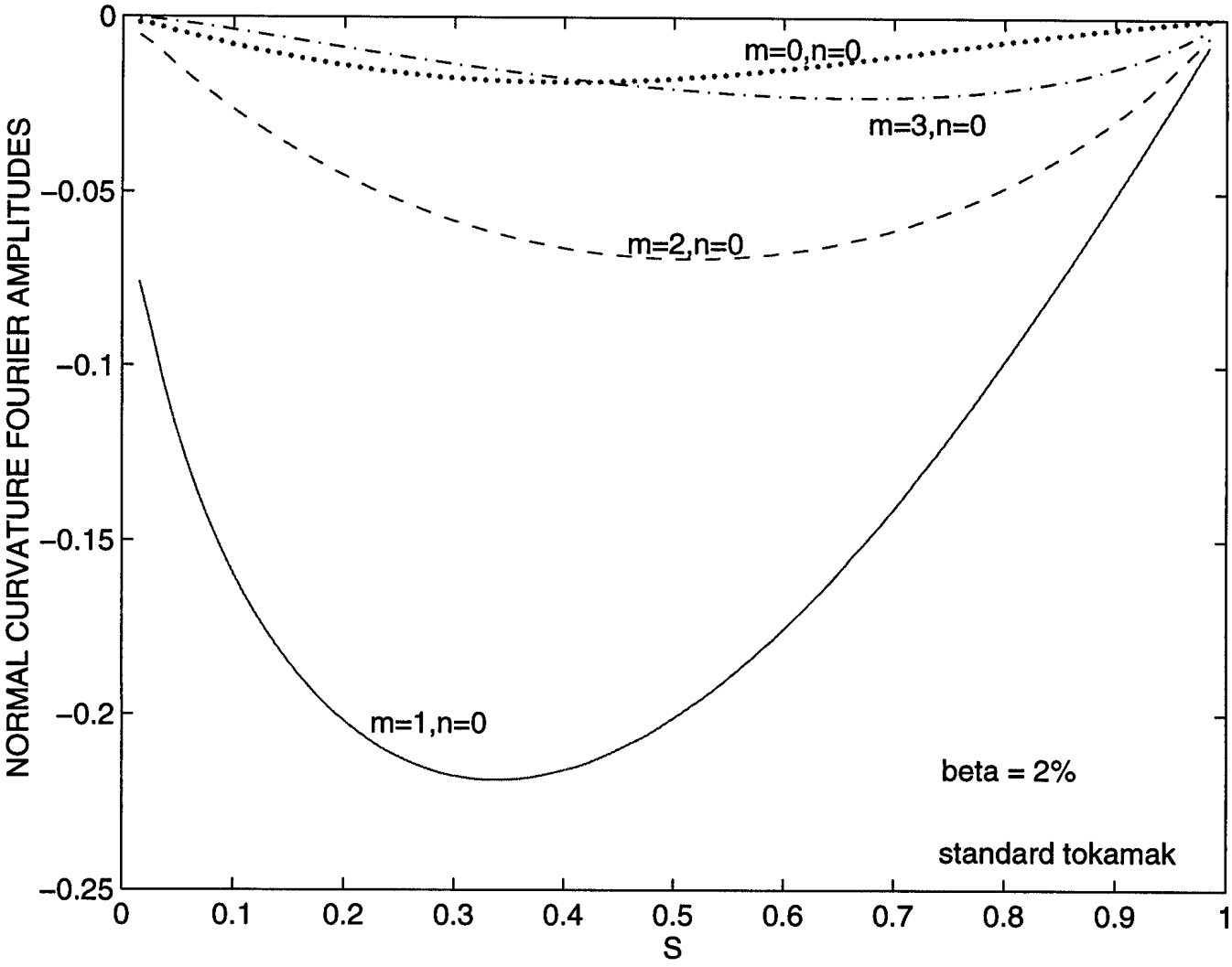

FIG. 3. The 4 principal Fourier amplitude profiles of $2p'(s)\sqrt{g}\kappa \cdot \nabla s$ as a function of s in a tokamak with conventional shear and inverse rotational transform varying from unity at the magnetic axis to 2.5 at the edge for $\beta = 2\%$.

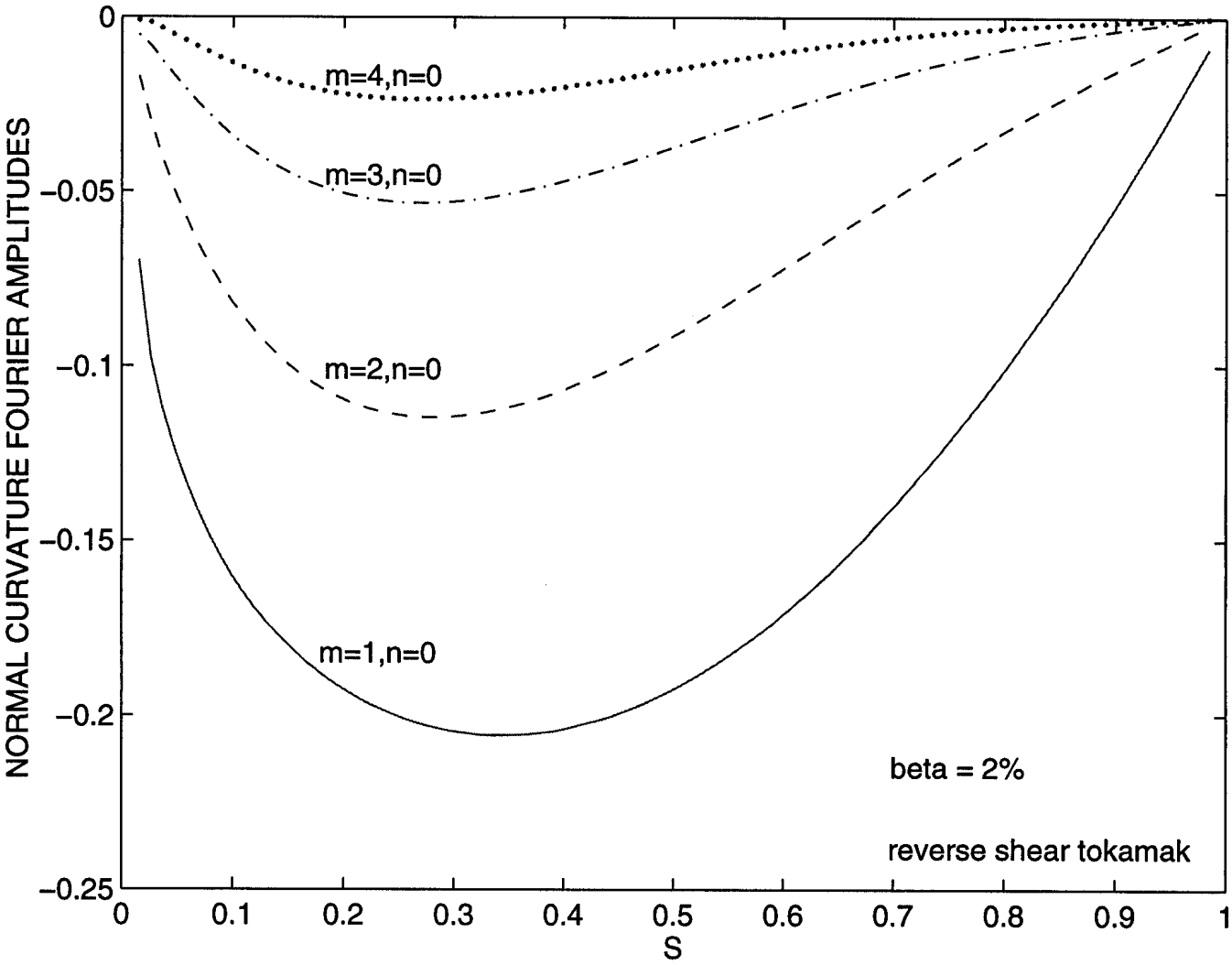

FIG. 4. The 4 principal Fourier amplitude profiles of $2p'(s)\sqrt{g}\kappa \cdot \nabla s$ as a function of s in a tokamak with reverse global magnetic shear that results from imposing the vacuum rotational transform profile of a 10 field period torsatron at $\beta = 2\%$.

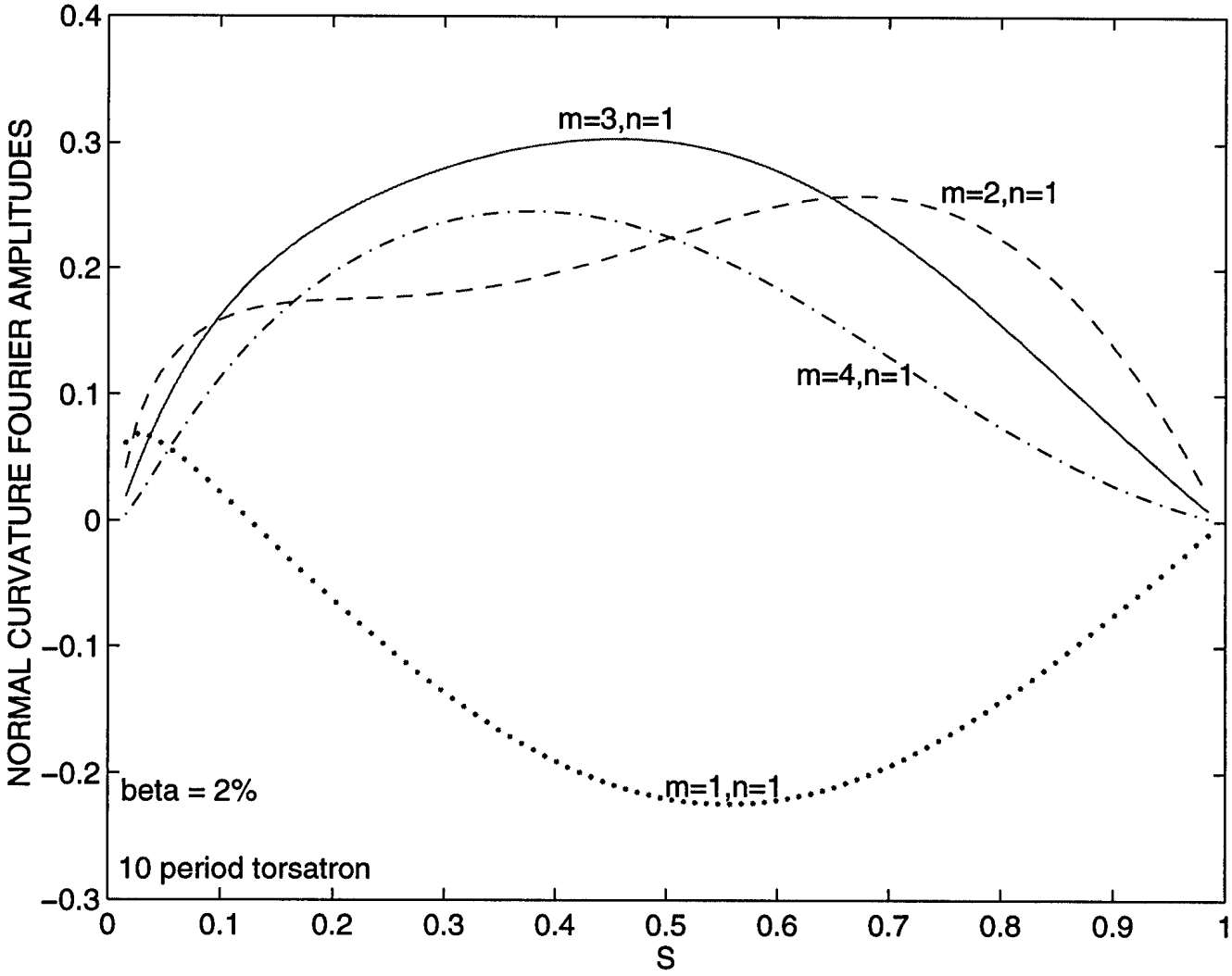

FIG. 5. The 4 principal Fourier amplitude profiles of $2p'(s)\sqrt{g}\kappa \cdot \nabla s$ as a function of s in a 10 field period torsatron with a fixed rotational transform profile that fits its vacuum equilibrium state at $\beta = 2\%$.

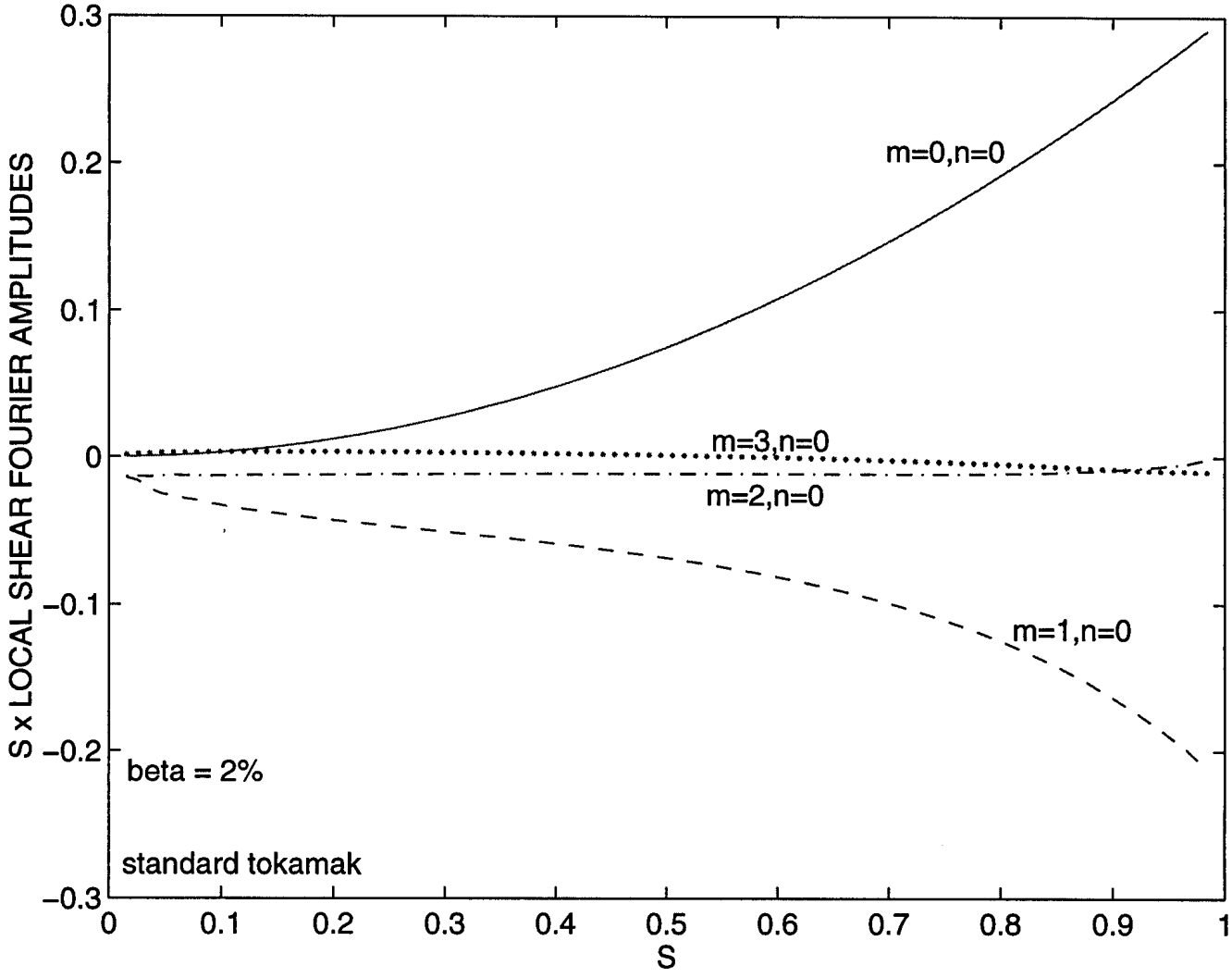

FIG. 6. The 4 principal Fourier amplitude profiles of $s\sqrt{g}S$ as a function of s in a tokamak with conventional shear and inverse rotational transform varying from unity at the magnetic axis to 2.5 at the edge for $\beta = 2\%$.

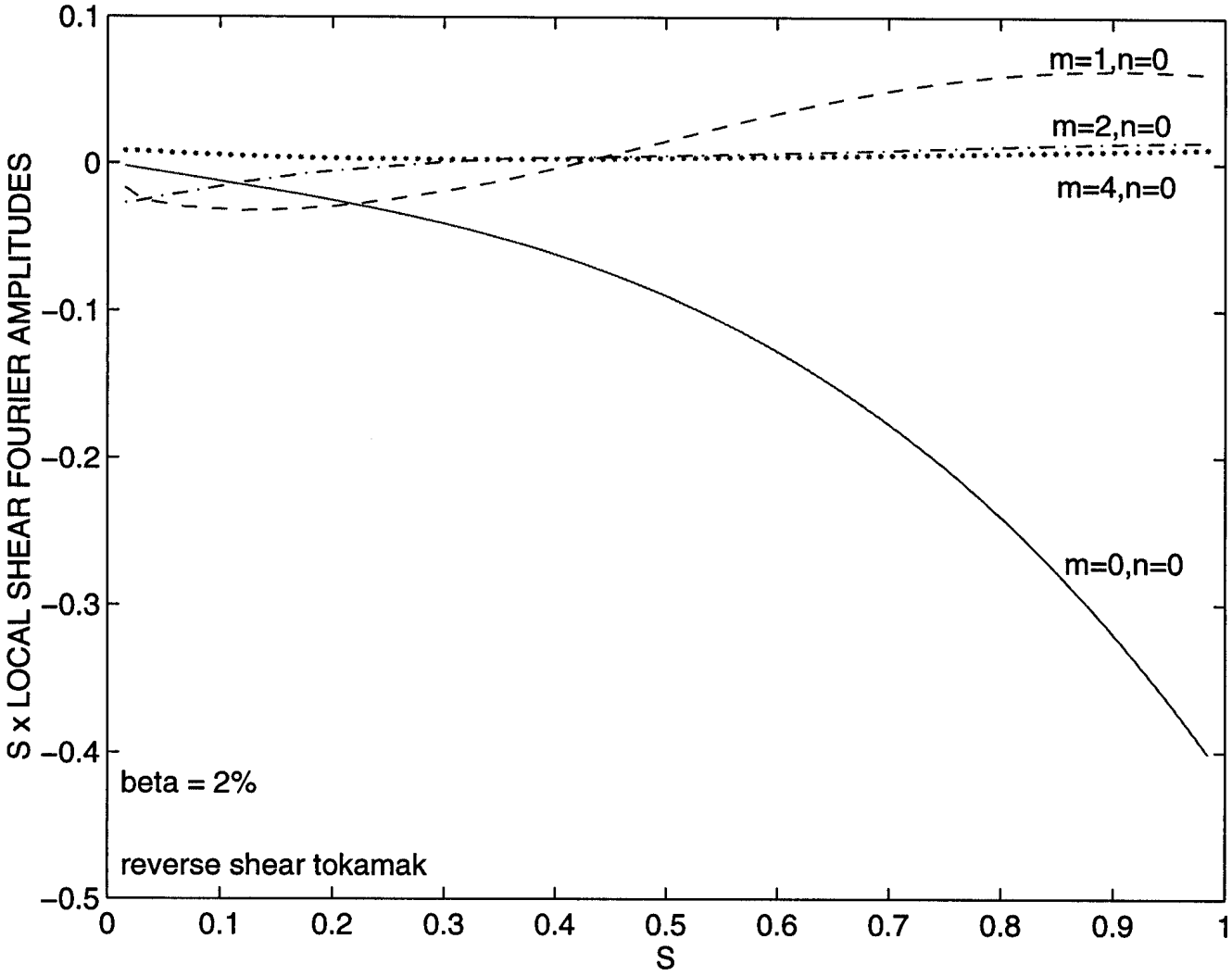

FIG. 7. The 4 principal Fourier amplitude profiles of $s\sqrt{g}S$ as a function of s in a tokamak with reverse global magnetic shear that results from imposing the vacuum rotational transform profile of a 10 field period torsatron at $\beta = 2\%$.

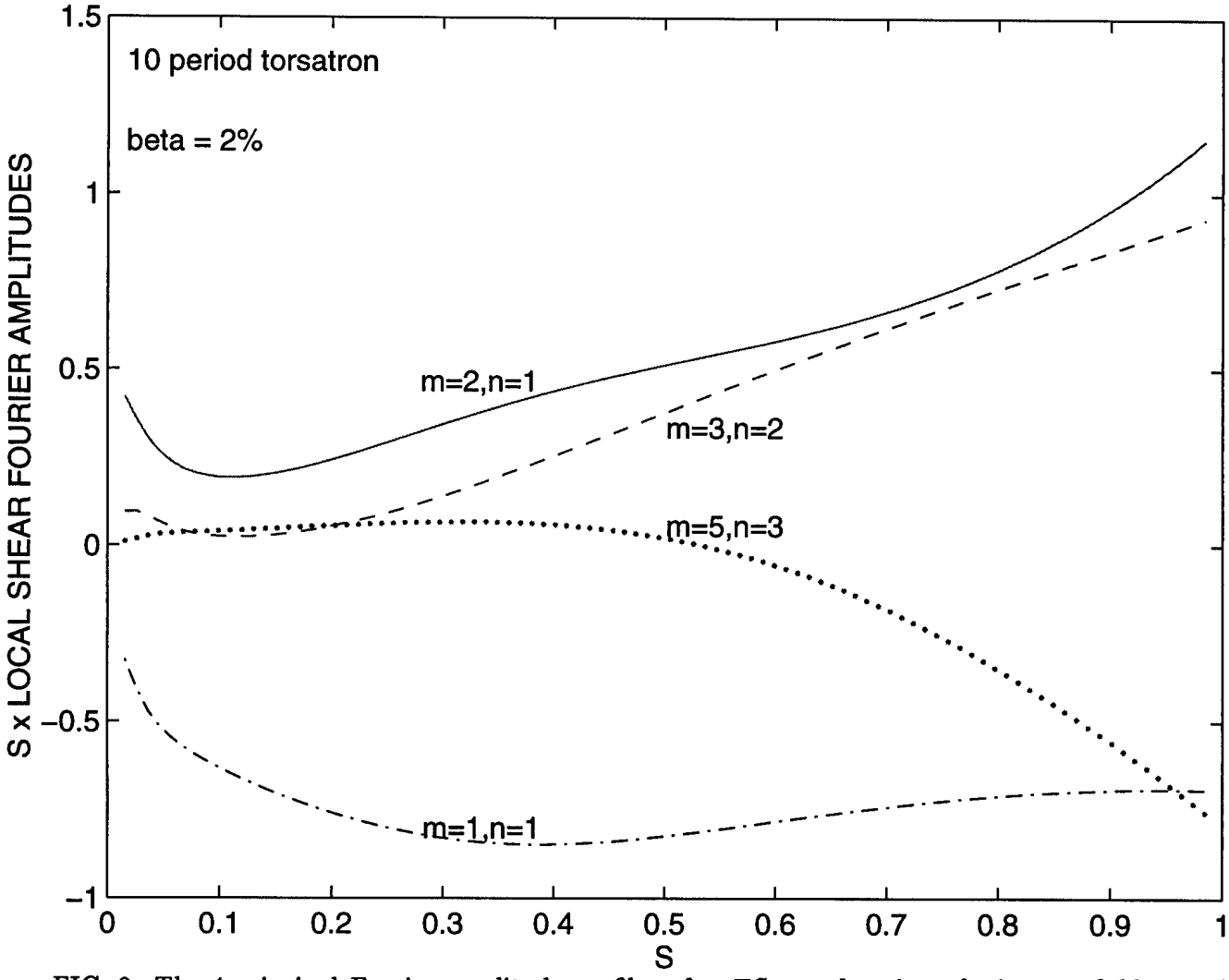

FIG. 8. The 4 principal Fourier amplitude profiles of $s\sqrt{g}S$ as a function of s in a 10 field period torsatron with a fixed rotational transform profile that fits its vacuum equilibrium state at $\beta = 2\%$.

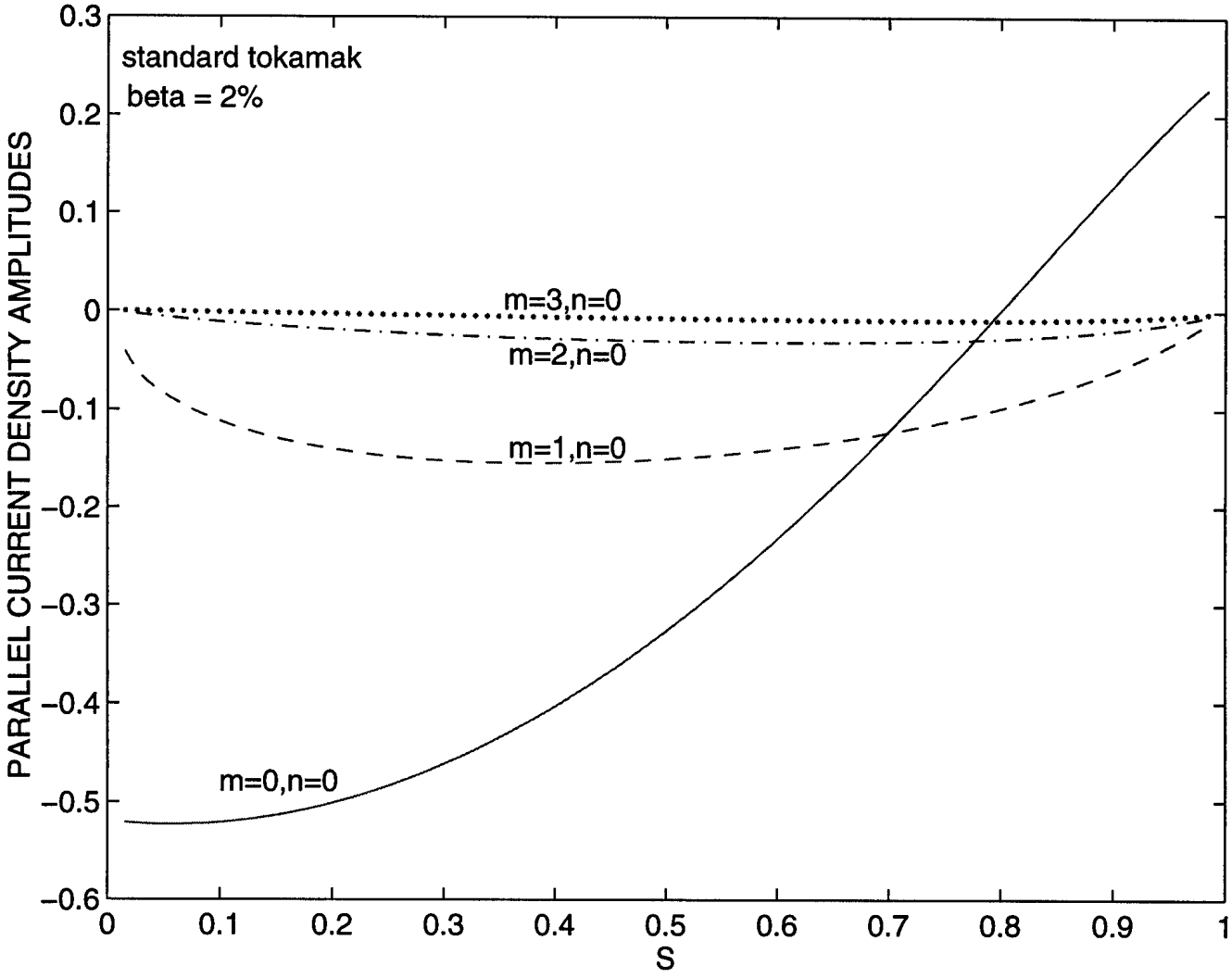

FIG. 9. The 4 principal Fourier amplitude profiles of $j \cdot B/B^2$ as a function of s in a tokamak with conventional shear and inverse rotational transform varying from unity at the magnetic axis to 2.5 at the edge for $\beta = 2\%$.

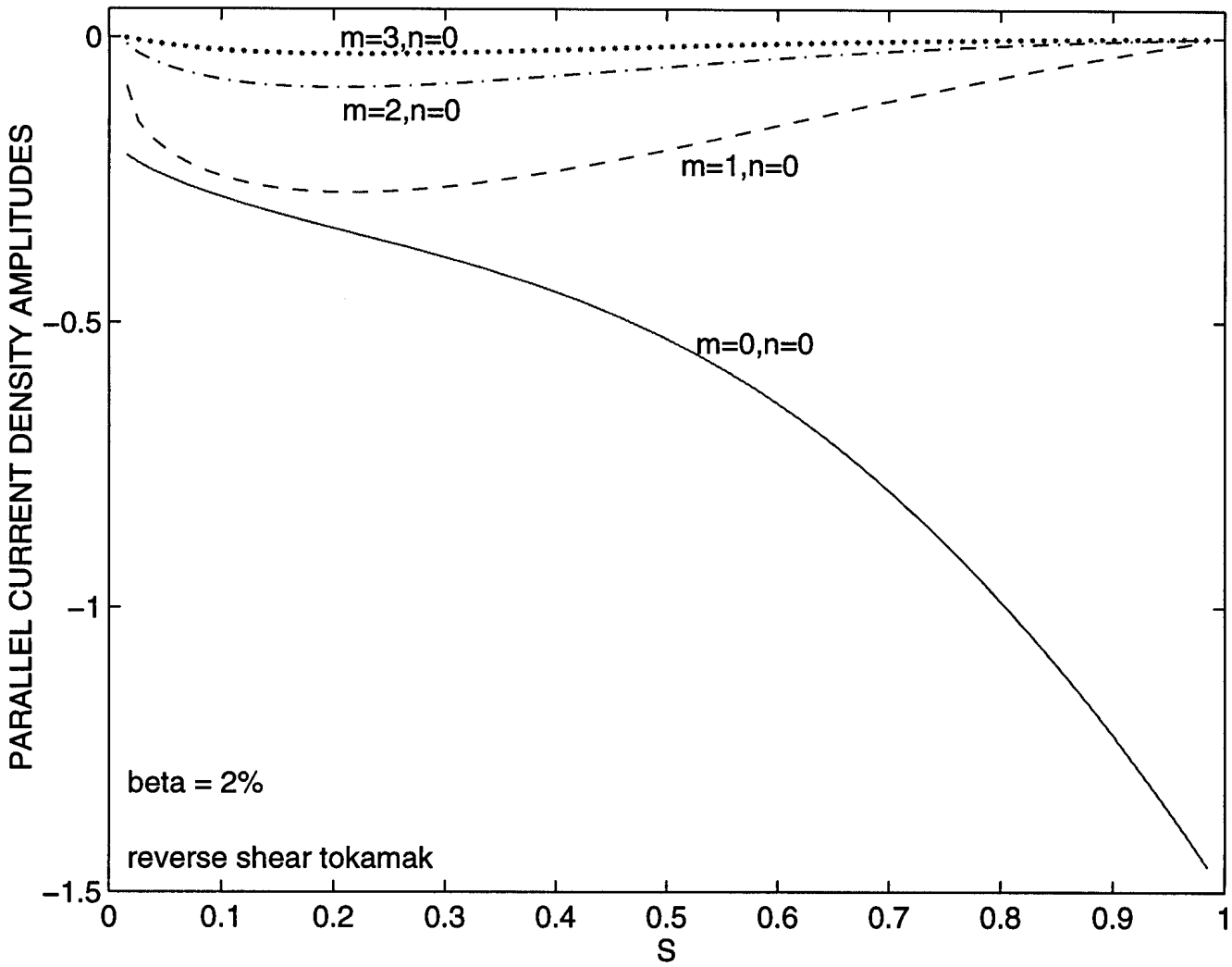

FIG. 10. The 4 principal Fourier amplitude profiles of $j \cdot B/B^2$ as a function of s in a tokamak with reverse global magnetic shear that results from imposing the vacuum rotational transform profile of a 10 field period torsatron at $\beta = 2\%$.

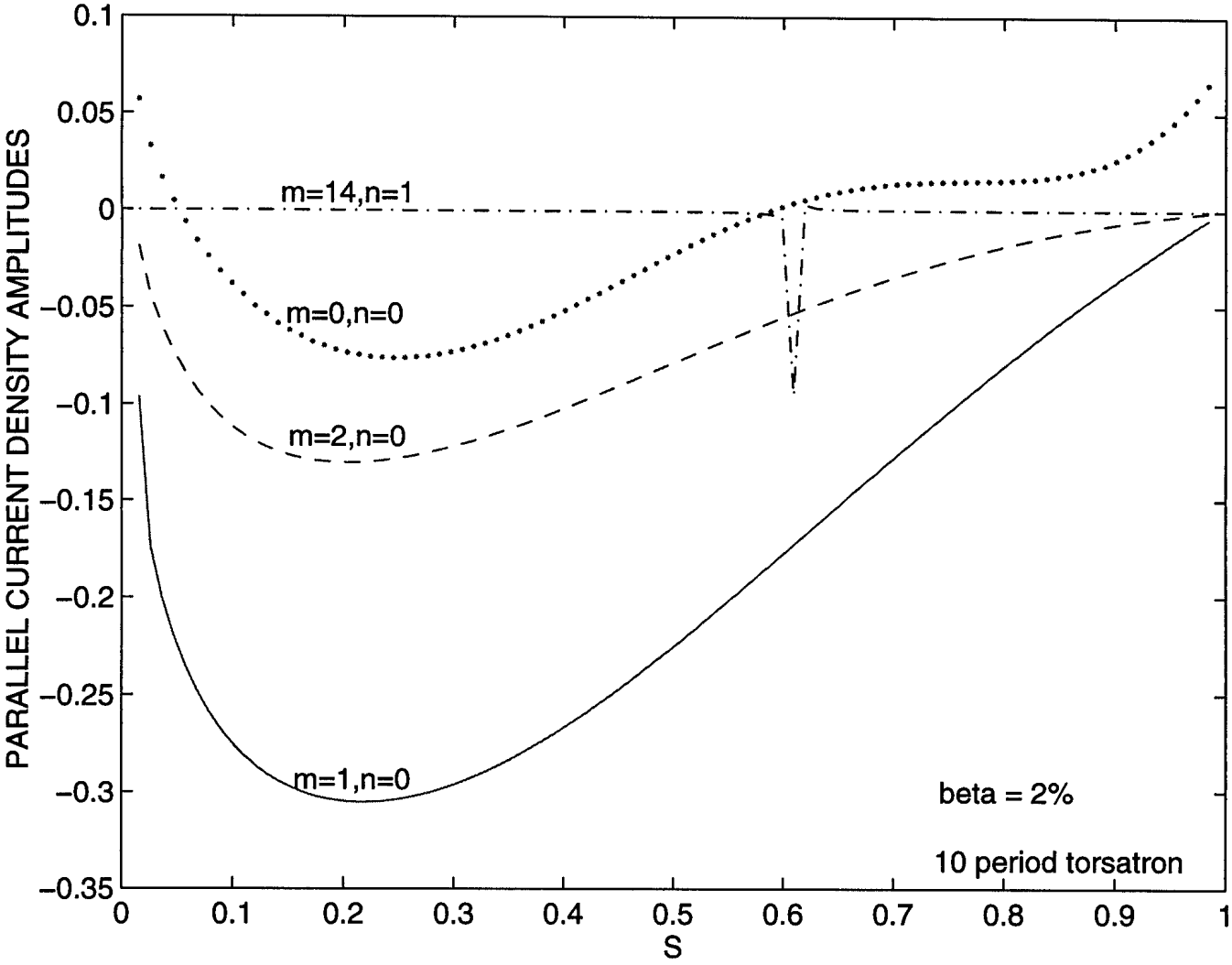

FIG. 11. The 4 principal Fourier amplitude profiles of $j \cdot B/B^2$ as a function of s in a 10 field period torsatron with a fixed rotational transform profile that fits its vacuum equilibrium state at $\beta = 2\%$.

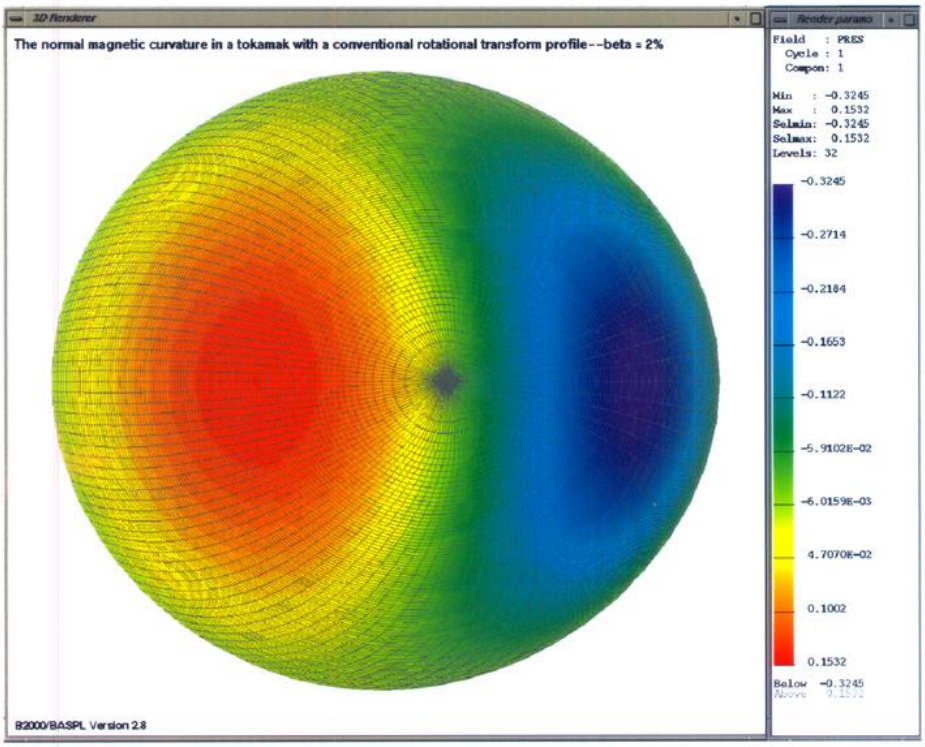

Fig. 12a. The distribution at $\beta = 2\%$ on a plane of constant Boozer coordinate toroidal angle of $2p'(s)\sqrt{g}\boldsymbol{\kappa} \cdot \boldsymbol{\nabla} s$ in a tokamak with conventional global magnetic shear and inverse rotational transform varying from unity at the magnetic axis to 2.5 at the edge. Shades of blue indicate the smallest/most negative values and shades of red indicate the largest/most positive values.

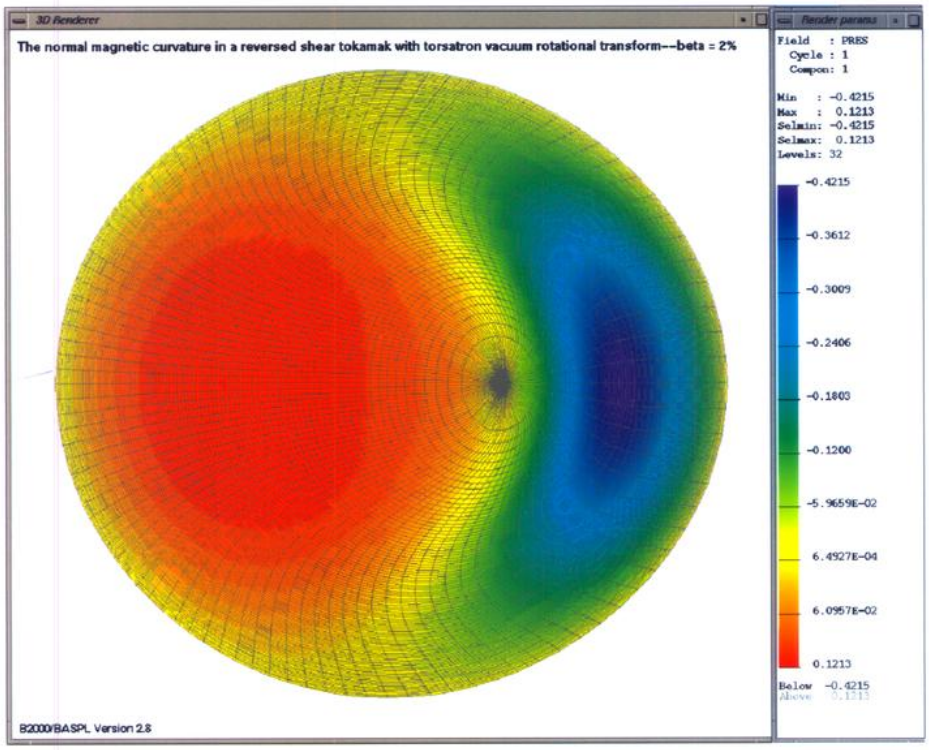

Fig. 12b. The distribution at $\beta = 2\%$ on a plane of constant Boozer coordinate toroidal angle of $2p'(s)\sqrt{g}\boldsymbol{\kappa} \cdot \boldsymbol{\nabla} s$ in a tokamak with reverse global magnetic shear that results from imposing the vacuum rotational transform profile of a 10 field period torsatron. Shades of blue indicate the smallest/most negative values and shades of red indicate the largest/most positive values.

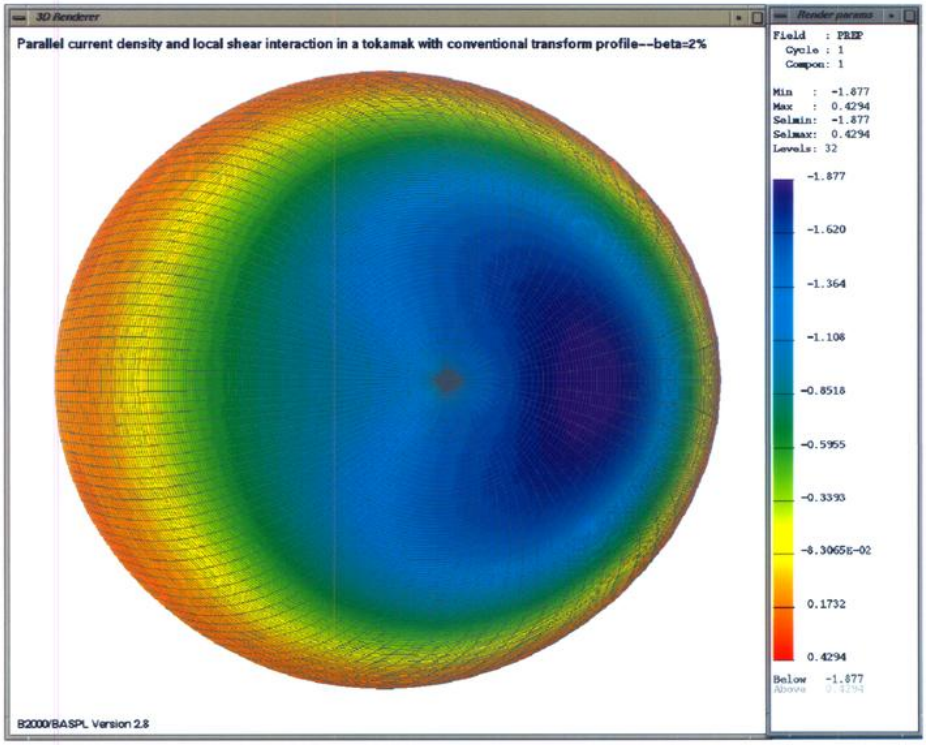

Fig. 12c. The distribution at $\beta = 2\%$ on a plane of constant Boozer coordinate toroidal angle of $\sigma(\sqrt{g}S|\nabla s|^2 + \sigma\sqrt{g}B^2)$ in a tokamak with conventional global magnetic shear and inverse rotational transform varying from unity at the magnetic axis to 2.5 at the edge. Shades of blue indicate the smallest/most negative values and shades of red indicate the largest/most positive values.

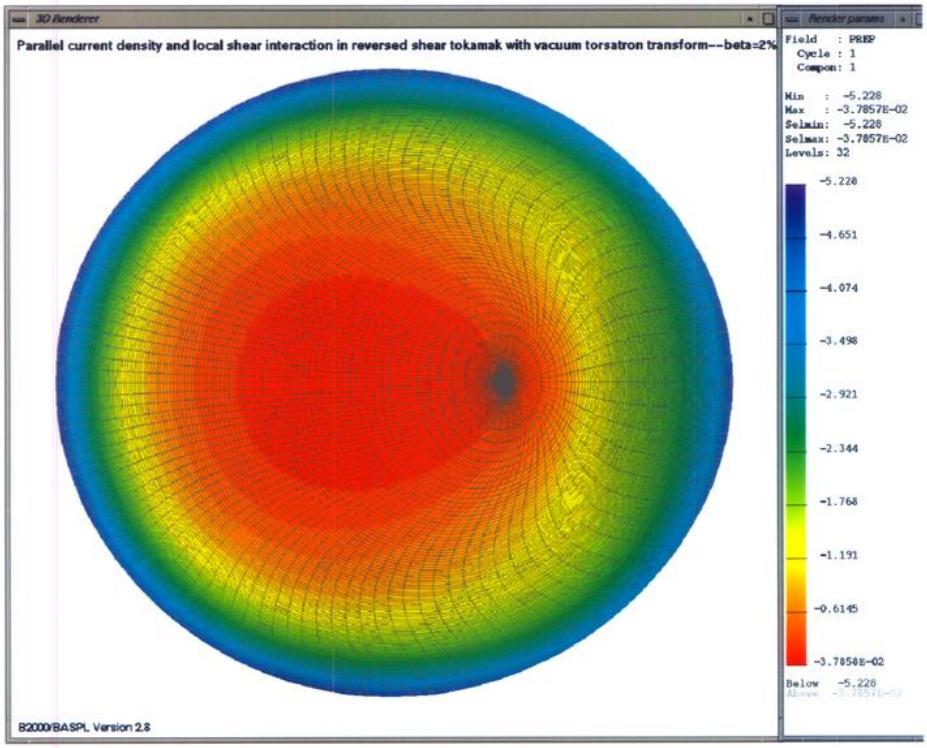

Fig. 12d. The distribution at $\beta = 2\%$ on a plane of constant Boozer coordinate toroidal angle of $\sigma(\sqrt{g}S|\nabla s|^2 + \sigma\sqrt{g}B^2)$ in a tokamak with reverse global magnetic shear that results from imposing the vacuum rotational transform profile of a 10 field period torsatron. Shades of blue indicate the smallest/most negative values and shades of red indicate the largest/most positive values.

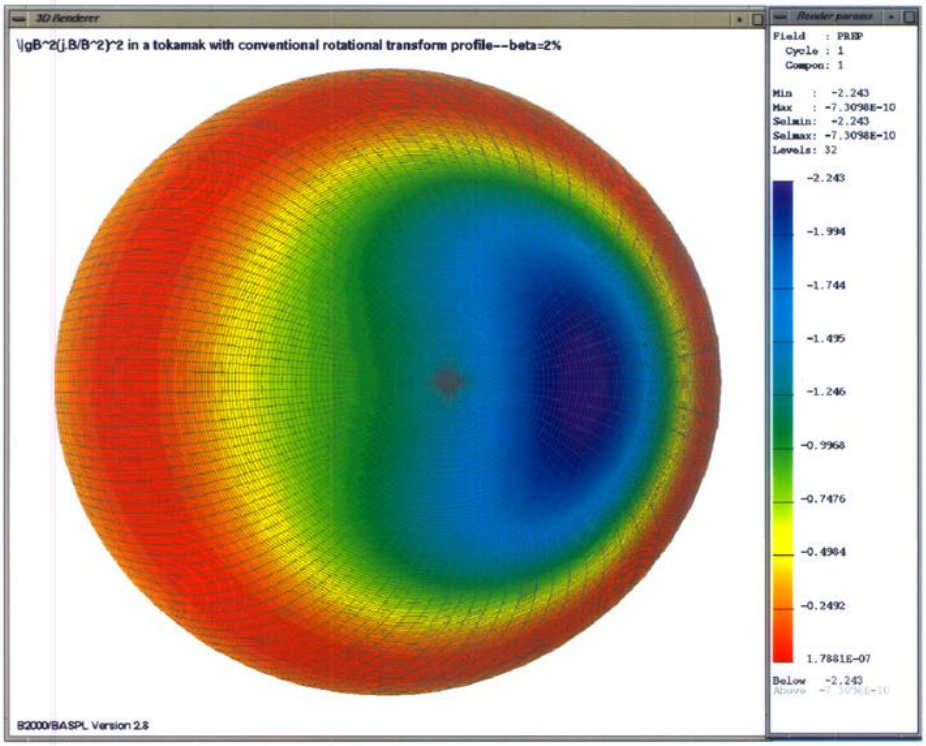

Fig. 12e. The distribution at $\beta = 2\%$ on a plane of constant Boozer coordinate toroidal angle of $\sigma^2\sqrt{g}B^2$ in a tokamak with conventional global magnetic shear and inverse rotational transform varying from unity at the magnetic axis to 2.5 at the edge. Shades of blue indicate the smallest/most negative values and shades of red indicate the largest/most positive values.

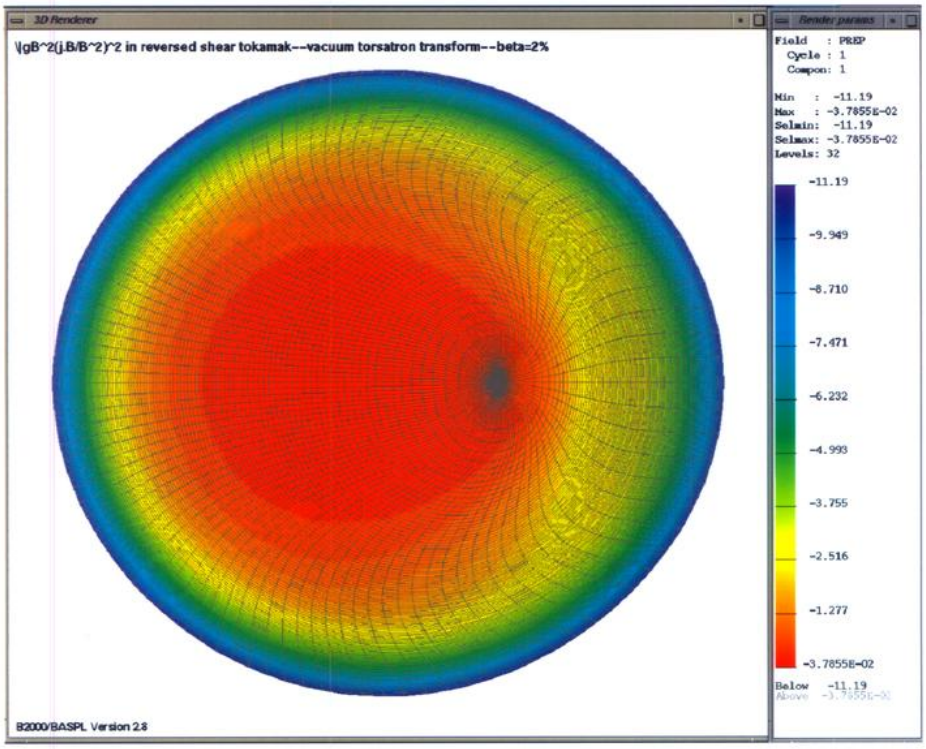

Fig. 12f. The distribution at $\beta = 2\%$ on a plane of constant Boozer coordinate toroidal angle of $\sigma^2\sqrt{g}B^2$ in a tokamak with reverse global magnetic shear that results from imposing the vacuum rotational transform profile of a 10 field period torsatron. Shades of blue indicate the smallest/most negative values and shades of red indicate the largest/most positive values.

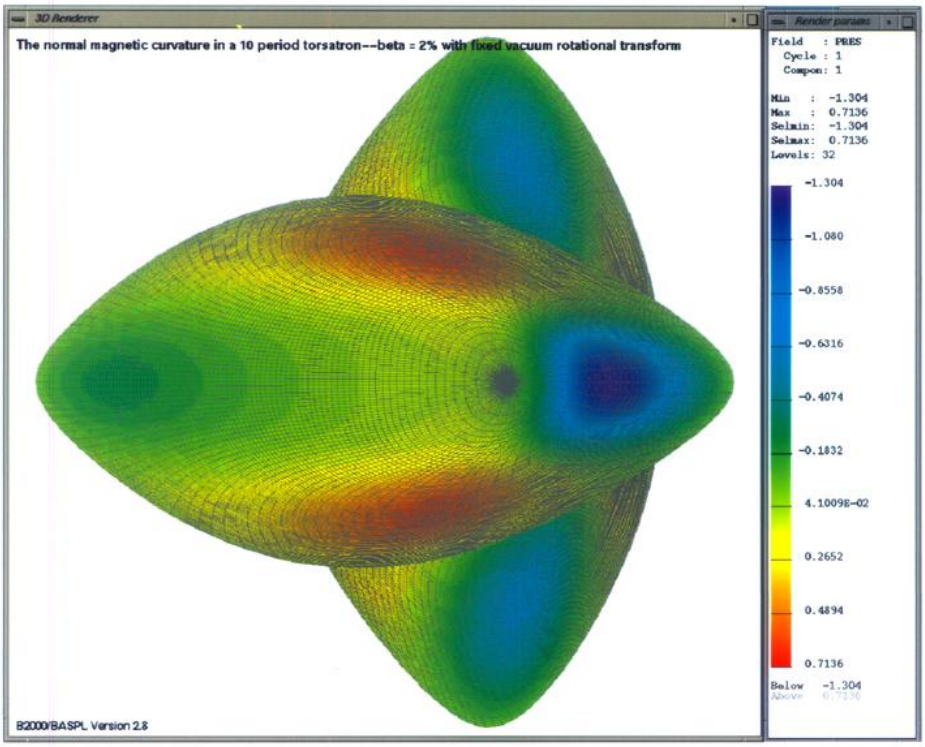

Fig. 13a. The distribution at $\beta = 2\%$ on the up-down symmetric planes of constant Boozer toroidal angle $\phi = \pi/10$ (foreground) and $\phi = 0$ (background) in a 10 field period torsatron with a fixed rotational transform profile that fits its vacuum equilibrium state of $2p'(s)\sqrt{g}\boldsymbol{\kappa} \cdot \boldsymbol{\nabla} s$. Shades of blue indicate the smallest/most negative values and shades of red indicate the largest/most positive values.

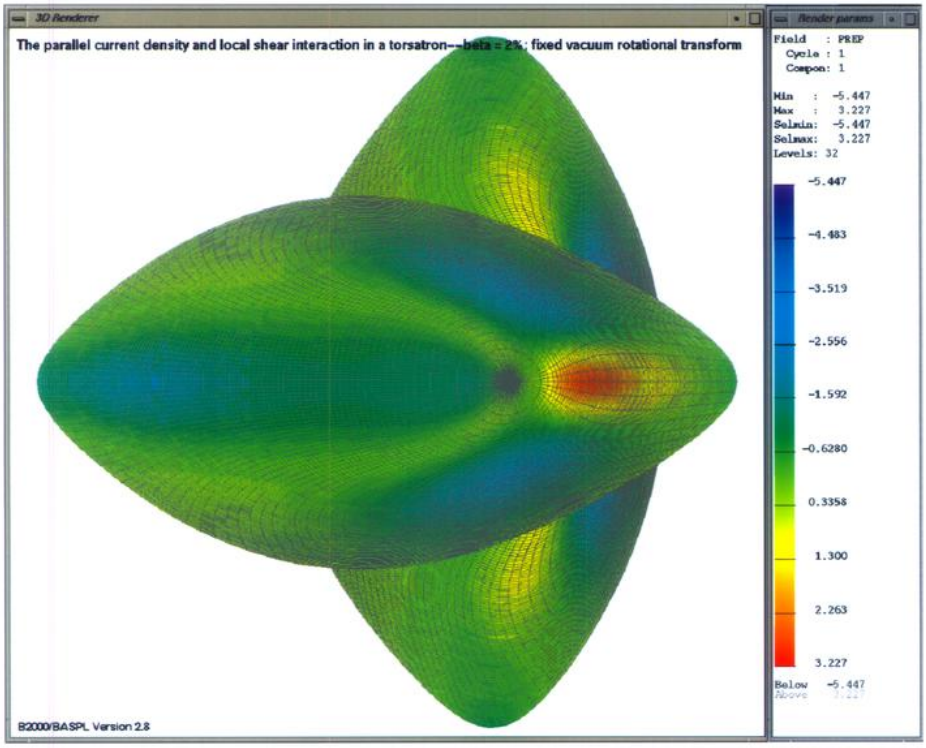

Fig. 13b. The distribution at $\beta = 2\%$ on the up-down symmetric planes of constant Boozer toroidal angle $\phi = \pi/10$ (foreground) and $\phi = 0$ (background) in a 10 field period torsatron with a fixed rotational transform profile that fits its vacuum equilibrium state of $\sigma(\sqrt{g}S|\boldsymbol{\nabla} s|^2 + \sigma\sqrt{g}B^2)$. Shades of blue indicate the smallest/most negative values and shades of red indicate the largest/most positive values.

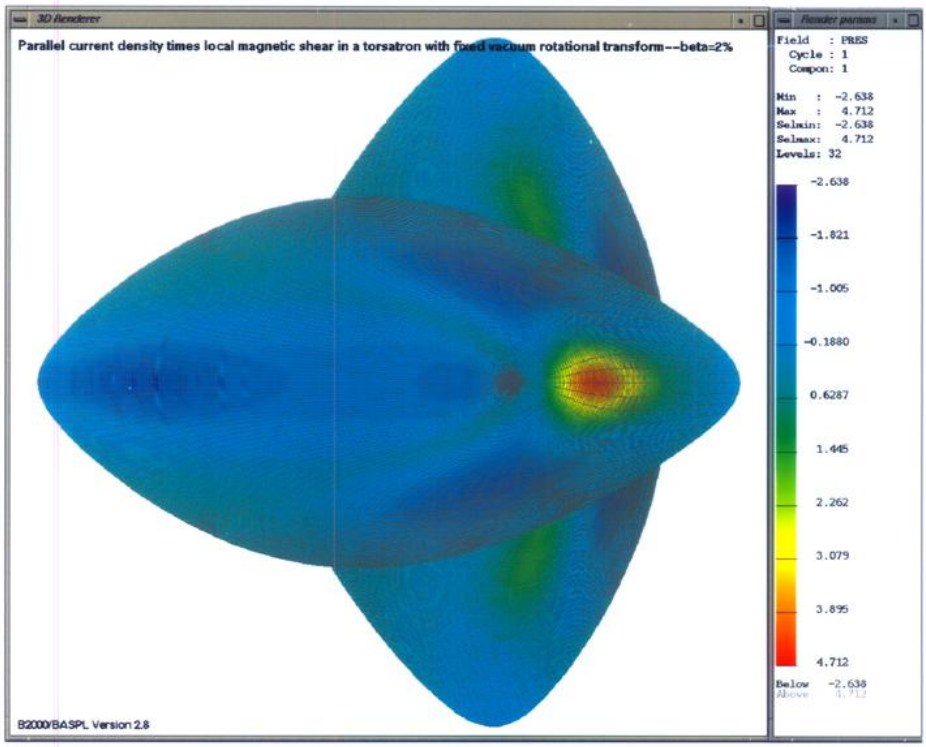

Fig. 13c. The distribution at $\beta = 2\%$ on the up-down symmetric planes of constant Boozer toroidal angle $\phi = \pi/10$ (foreground) and $\phi = 0$ (background) in a 10 field period torsatron with a fixed rotational transform profile that fits its vacuum equilibrium state of $\sigma\sqrt{g}S|\nabla s|^2$. Shades of blue indicate the smallest/most negative values and shades of red indicate the largest/most positive values.

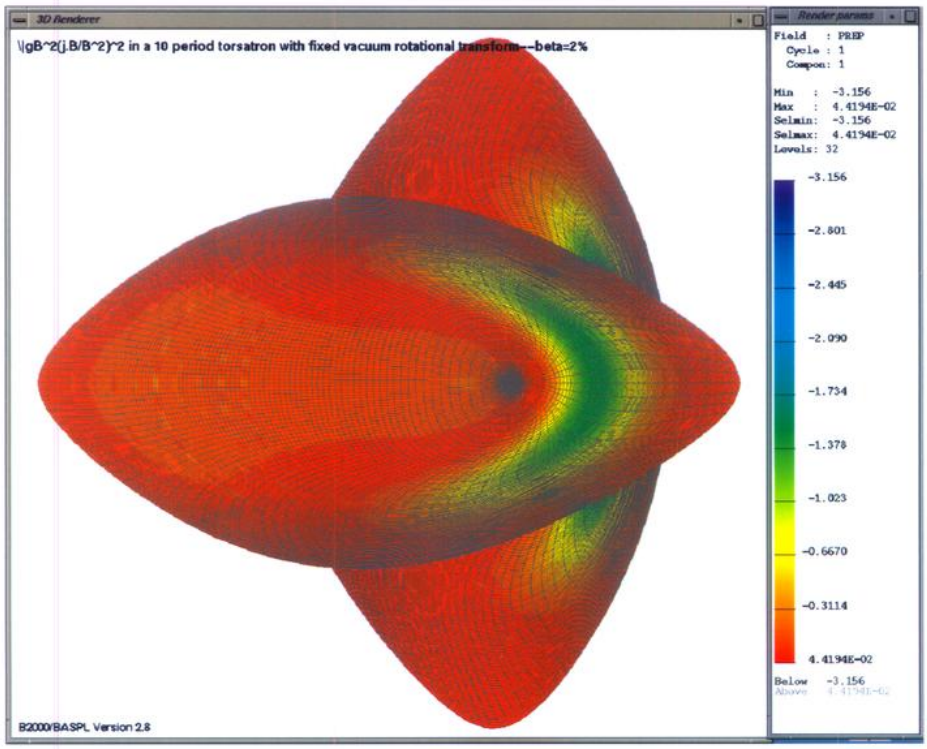

Fig. 13d. The distribution at $\beta = 2\%$ on the up-down symmetric planes of constant Boozer toroidal angle $\phi = \pi/10$ (foreground) and $\phi = 0$ (background) in a 10 field period torsatron with a fixed rotational transform profile that fits its vacuum equilibrium state of $\sigma^2\sqrt{g}B^2$. Shades of blue indicate the smallest/most negative values and shades of red indicate the largest/most positive values.

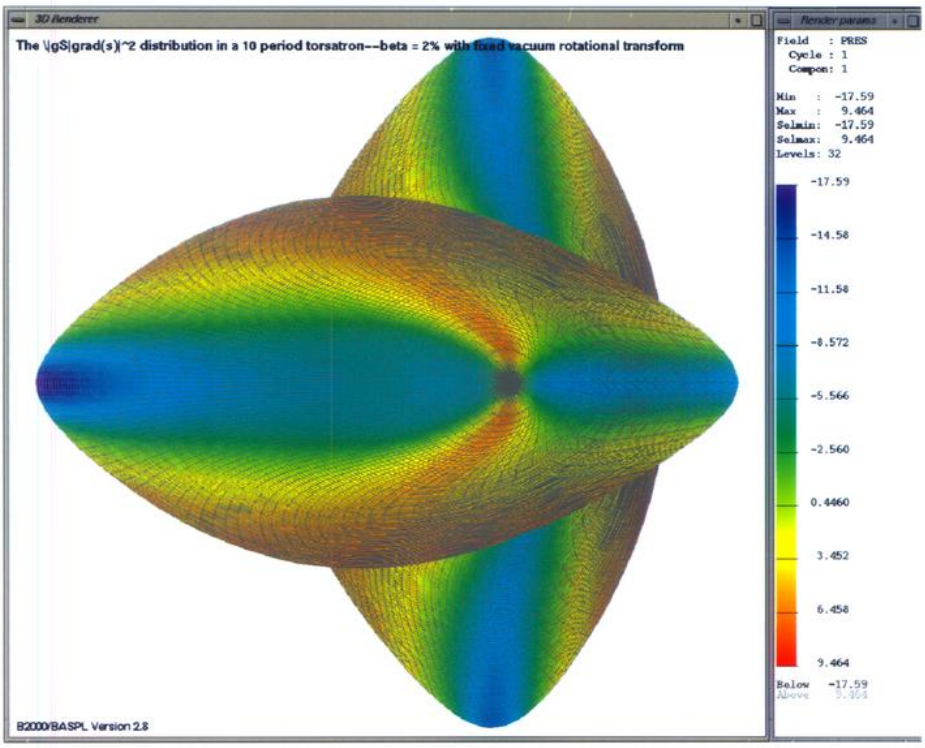

Fig. 13e. The distribution at $\beta = 2\%$ on the up-down symmetric planes of constant Boozer toroidal angle $\phi = \pi/10$ (foreground) and $\phi = 0$ (background) in a 10 field period torsatron with a fixed rotational transform profile that fits its vacuum equilibrium state of $\sqrt{g}S|\nabla s|^2$. Shades of blue indicate the smallest/most negative values and shades of red indicate the largest/most positive values.

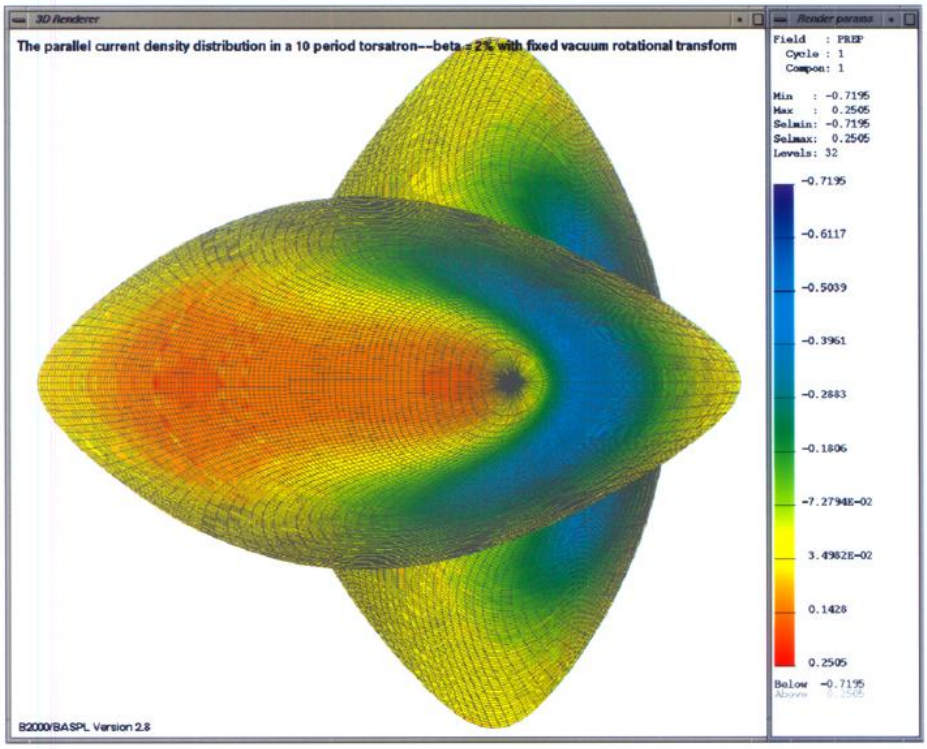

Fig. 13f. The distribution at $\beta = 2\%$ on the up-down symmetric planes of constant Boozer toroidal angle $\phi = \pi/10$ (foreground) and $\phi = 0$ (background) in a 10 field period torsatron with a fixed rotational transform profile that fits its vacuum equilibrium state of the parallel current density σ. Shades of blue indicate the smallest/most negative values and shades of red indicate the largest/most positive values.